HHS Public Access

Author manuscript

Auton Neurosci. Author manuscript; available in PMC 2023 September 18.

Published in final edited form as:

Auton Neurosci. 2014 April ; 181: 37–48. doi:10.1016/j.autneu.2013.12.010.

Distribution and Morphology of Calcitonin Gene-Related Peptide and Substance P Immunoreactive Axons in the Whole-Mount Atria of Mice

Liang Li[1,*], **Jeffrey T. Hatcher**[1,*], **Donald B. Hoover**[2], **He Gu**[3], **Robert D. Wurster**[4], **Zixi (Jack) Cheng**[1,#]

[1]Biomolecular Science Center, Burnett School of Biomedical Sciences, College of Medicine, University of Central Florida, Orlando, FL 32816

[2]Department of Biomedical Sciences, Quillen College of Medicine, East Tennessee State University, Johnson City, TN 37614

[3]Department of Anesthesia, University of Iowa Hospital and Clinics, Iowa City, IA 52242

[4]Department of Physiology, Loyola University, Stritch School of Medicine, Maywood, IL 60153

Abstract

The murine model has been used to investigate the role of cardiac sensory axons in various disease states. However, the distribution and morphological structures of cardiac nociceptive axons in normal murine tissues have not yet been well characterized. In this study, whole-mount atria from FVB mice were processed with calcitonin gene-related peptide (CGRP) and substance P (SP) primary antibodies followed by secondary antibodies, and then examined using confocal microscopy. We found: 1) Large CGRP-IR axon bundles entered the atria with the major veins, and these large bundles bifurcated into small bundles and single axons that formed terminal end-nets and free endings in the epicardium. Varicose CGRP-IR axons had close contacts with muscle fibers, and some CGRP-IR axons formed varicosities around principle neurons (PNs) within intrinsic cardiac ganglia (ICGs). 2) SP-IR axons also were found in the same regions of the atria, attached to veins, and within cardiac ganglia. Similar to CGRP-IR axons, these SP-IR axons formed terminal end-nets and free endings in the atrial epicardium and myocardium. Within ICGs, SP-IR axons formed varicose endings around PNs. However, SP-IR nerve fibers were less abundant than CGRP-IR fibers in the atria. 3) None of the PNs were CGRP-IR or SP-IR. 4) CGRP-IR and SP-IR often colocalized in terminal varicosities around PNs. Collectively, our data document the distribution pattern and morphology of CGRP-IR and SP-IR axons and terminals in different regions of the atria. This knowledge provides useful information for CGRP-IR and SP-IR axons that can be referred to in future studies of pathological remodeling.

[#]Correspondance to: Zixi (Jack) Cheng, Ph.D., BMS Building 20, Room 230, Biomolecular Science Center, Burnett School of Biomedical Sciences, College of Medicine, University of Central Florida, 4000 Central Florida Blvd, Orlando, FL 32816. Tel: (407) 823 1505; Fax: (407) 823 0956, zcheng@mail.ucf.edu.

[*]The first two authors equally contributed to this work.

Keywords

Neuropeptides; CGRP; SP; Nociceptive; Atria; Cardiac ganglia

INTRODUCTION

The murine models have often been used as an experimental model to investigate cardiac nerve innervation in health and disease. In particular, mice have been previously used to study diabetes-induced cardiac sensory neuropathy (Ieda et al., 2006; Song et al., 2007; Wei et al., 2009) as well as calcitonin gene-related peptide (CGRP) and substance P (SP) modulation of heart rate (Kunz et al., 2007) and coronary blood flow (Hongbao et al., 2009). However, prior studies have relied on slice-preparations, radioimmunoassay, or western-blot assay. Therefore, the distribution and morphology of afferent axons and terminals have not yet been well documented. This gap in knowledge has impeded the progress of focused investigation on disease-induced pathological changes of nociceptive afferent cardiac nerves. The goal of the present study was to investigate the distribution and structural features of CGRP and SP axons and terminals in whole-mount atrial tissues of mice in order to establish normal patterns of afferent fiber innervation of atria.

CGRP and SP are both peptidergic neurotransmitters in capsaicin-sensitive sensory nerves (Holzer, 1991; Maggi, 1995). The dorsal root ganglia contain both CGRP and SP sensory neurons, which project centrally to the dorsal horn in the spinal cord for pain sensation and peripherally to the heart (atria and ventricles) and other organs to detect the chemical signals (e.g., bradykinin) that are released during myocardial injury. These damage signals are transduced through a transient receptor potential involving vanilloid (TRPV1)-mediated mechanisms, to induce neurogenic responses (Zahner et al., 2003; Pan and Chen, 2004; Geppetti et al., 2008; Benemei et al., 2009; Thornton et al., 2010). The stimuli that lead to the sensation of pain are detected by spinal afferent terminals within the heart (Pan and Chen 2004).

Structure and function of CGRP-IR and SP-IR neurons and axons have been examined in several different species such as humans, dogs, cats, guinea pigs, rats, and mudpuppies (Saito et al., 1986; Parsons and Neel, 1987; Papka and Urban, 1987; Richardson et al., 2003; Hoover et al., 2008, 2009; Mousa et al., 2010). However, most of these studies used sectioned cardiac tissues in which the continuity of axon and terminal structures has been largely disrupted, leading to a *partial* view of the innervation pattern in the atria. Although whole-mount cardiac tissues were used in some studies, these studies mainly focused on some special cardiac targets, such as cardiac ganglia (Richardson et al., 2003; Parsons et al., 2004). Thus far, no studies of CGRP-IR and SP-IR cardiac axons and terminals have been reported in mouse atria. The size and tissue characteristics of the mouse heart make it amenable to whole-mount studies of cardiac nerve distribution. This study provides a comprehensive, holistic (3-D) characterization of these fibers, thus providing more information than previous studies of sectioned cardiac tissues in other species. CGRP and SP were chosen as representative markers of nociceptive nerve types, and their peptidergic nature makes them good targets for antibody probes. Therefore, the goal of the

present study was to learn the distribution, and morphology of CGRP and SP axons and terminals in the whole-mount atria of mice. Previously, we have studied distribution and morphology of parasympathetic afferent and efferent axons in the atria and aortic arch in normal animals (Cheng et al., 1997a,b; 2004; Cheng and Powley 2000; Ai et al., 2007a) as well as later in disease models (e.g., aging, sleep apnea, and diabetes) (Ai et al.,2007b; 2009; Lin et al., 2008; Li et al., 2010). The present study extends this database by documenting the distribution and morphology of CGRP and SP axons and terminals in whole-mount atria of mice.

MATERIALS AND METHODS

Animals

Male FVB (FVB/N in full name) mice (n=20, age 3 – 6 months) were used for this study. The FVB strain has been used for producing transgenic mice because it has easy to inject pronuclei at the single cell stage and it is a healthy, fertile breeder (Epstein et al. 1989, Zheng et al. 2011). The transgenic line of OVE26 diabetic mice was originally constructed on the inbred strain FVB. We have used OVE26 diabetic mice to study diabetes and maternal diabetes-induced cardiac neuropathy (Gu et al. 2008, 2009, Yan 2009, Li et al. 2010, Lin et al. 2010a,b, 2011). All animals were housed in a room in which light/dark cycles were set to 12 h/12 h (6:00 AM to 6:00 PM light cycle) and provided food and water ad libitum. All procedures were approved by the University of Central Florida Animal Care and Use Committee and strictly followed the guidelines established by NIH. All experiments conformed to the University of Central Florida guidelines on the ethical use of animals.

Tissue Preparation

Mice were anesthetized with a lethal dose of sodium pentobarbital (i.p., 100 μg/g). Absence of the hind paw pinch withdrawal reflex was used as an indicator to ensure sufficient depth of anesthesia. Mice were perfused through the left ventricle with 40° C phosphate-buffered saline (0.1 M PBS, pH=7.4) for 5 minutes. The inferior vena cava was cut to drain the blood and perfusate. Tissues were then fixed by perfusion with 4° C Zamboni's fixative (15% picric acid and 2% paraformaldehyde in PBS, pH=7.4). The heart and lungs were removed together with the trachea and the esophagus to ensure inclusion of all cardiac tissues. These specimens were post-fixed in 4° C Zamboni's fixative for 8–24 hours.

After postfixation, the heart and lungs were dissected apart. Briefly, the pulmonary veins were separated from the lungs with fine tweezers, and the lungs and trachea were discarded. Atria were separated from the ventricles with fine scissors along the atrioventricular groove, and the aortic arch was then separated from the atria. The right and left atria were separated along the interatrial septum. The dissected specimens are as follows: 1) right atrium with the inferior vena cava (IVC), superior vena cava (SVC) and left precaval vein (LP-CV) attached and 2) left atrium with pulmonary veins (PVs) attached (Cheng et al., 1997a; Ai et al.,2007a).

Following postfixation, the duodenum was removed, washed using tap water and cut open along the mesenteric attachment. A 2 cm long sheet of duodenal muscle wall near the

pylorus was prepared as wholemounts after the submucosal/mucosal layers were separated from the muscle wall with forceps (Fox et al. 2000). This muscle wall contained longitudinal and circular muscle layers with the myenteric nervous system embedded between them. Wholemounts of the muscle wall were processed with SP and CGRP antibodies as described above for the atrial tissue.

Immunohistochemistry

All immunohistochemical procedures were performed on a shaker at room temperature (~22–24° C) in a 24-well plate. Dissected tissues were washed six times for 5 minutes in 0.01 M PBS pH=7.4 to remove the remaining fixative. Tissues were then blocked 5 days in a blocking mixture containing 2% bovine serum albumin, 10% normal donkey serum, 0.08% Triton X-100, and 0.08% $NaNH_3$ in 0.01 M PBS, pH=7.4, followed by a 24 hour primary antibody incubation (CGRP, 1:1000; Substance P, 1: 500) in a solution comprising 2% bovine serum albumin, 4% normal donkey serum, 0.08% Triton X-100, and 0.05% NaN_3 in 0.01 M PBS, pH=7.4). The tissues were thoroughly washed six times for 5 minutes in PBST (0.4% Triton X-100 in 0.01 M PBS) to remove unbound primary antibodies. Tissues were then kept in the dark and incubated in a fluorescent secondary antibody solution (1:500 in PBST, Table 1) for 2 h. Unbound secondary antibodies were removed by washing six times for 5 minutes in PBS. Negative controls performed without primary antibodies presented no immunoreactivity, confirming that nonspecific binding of secondary antibodies did not occur.

Tissues were then mounted onto glass slides, flatten with lead weights (6.75 Kg) for 1 h, and air-dried under a fume hood for 1 h. Slides were dehydrated by immersion for 2 minutes in each of 4 ascending concentrations of ethanol (75%, 95%, 100% and 100%), followed by two10 min immersions in 100% xylene. Cover glasses were then attached using DEPEX mounting medium (Electron Microscopy Sciences #13514) and allowed to dry overnight.

Data collection and analysis

Slides were examined using a Leica SP5 laser scanning confocal microscope with HeNe laser to detect CGRP-IR (543 nm) and SP-IR (633 nm) in the atrial whole-mounts. An argon-krypton laser (488nm) was used to detect background autofluorescence of the tissues (e.g., cardiac muscles and ganglionic cells). The confocal projection images for assembling montages of the atria were scanned using a 20x oil immersion objective lens (zoom X1). To show detailed CGRP-IR and SP-IR axon distribution in the heart, confocal optical sectioned images were scanned using a 40x oil immersion objective lens (zoom X2). All confocal images were scanned with similar settings. Modifications, including brightness and contrast adjustments, cropping and scale bar additions, were conducted utilizing Photoshop or NIH ImageJ (Collins 2007) software. Confocal montages were assembled using the landmark-based method for efficient, robust, and automated computational synthesis of high-resolution, wide-area images of a specimen from a series of overlapping partial views (Becker et al., 1996). Individual scans of a small image window were first obtained and saved in stacks of optical sectioned images. Then, these stacks were maximally-projected to yield a series of all-in-focus maximum projection tiles. MosaicJ (Thévenaz and Unser, 2007) was utilized to assist in the assembly of these tiles to create large montage images.

RESULTS

Distribution and morphology of CGRP-IR axons and terminals in whole-mount atria

The whole-mount nature of atrial preparations allowed for the assessment of CGRP-IR axon innervation in the right and left atria of mice (Fig. 1A & 1B). Although variations in structural details were observed across animals, the general scheme of CGRP-IR nerve distribution was similar in all animals studied. This is shown in a schematic drawing based on images collected from the representative mouse (Fig. 2). In both right and left atria (Figs 1A & 1B), large bundles of CGRP-IR axons entered the atria. The large bundles bifurcated multiple times into fine individual axons, which formed extensive terminal end-nets and free endings over the entire atria including the auricles and the entrance areas of several major veins (Figs. 3 & 4). The axon terminals were mostly in the epicardium and the underlying myocardium (Fig. 4).

As previously reported, 15–20 intrinsic cardiac ganglia of different sizes (Ai et al., 2007a; Lin et al., 2008) were found in the dorsal surface of the right and left atria (Fig 2). CGRP fibers traveled in the nerve bundles connecting these ganglia (Figs. 2 and 5). Some CGRP-IR axons formed varicose endings around individual principal neurons (PNs) of the intrinsic cardiac ganglia (ICG), whereas other varicose fibers appeared to pass by the ICG (Fig. 5). CGRP immunoreactivity was observed in numerous nerve fibers within the ganglia but was not found within the somata of PNs. The distribution and morphology of CGRP-IR axons in the right and left atria are shown in Figure 2.

Distribution and morphology of SP-IR axon and terminals in whole-mount atria

Similar to CGRP-IR innervation of the atria, we found that several large SP-IR axon bundles entered the atria and bifurcated into smaller bundles (Fig. 6A). Axons, terminal end-nets and free endings were seen in all regions of the atria and in associated veins (e.g., Figs. 6B–6E). In addition, varicose terminals occurred around some PNs (Fig .6F). SP-IR axons and terminals were less abundant compared to the labeling observed for CGRP (Figs. 3–4).

Colocalization of CGRP-IR and SP-IR innervation in the atria

SP-IR (red) fibers also demonstrated CGRP (green) immunoreactivity (Figs. 7A–7B). Within cardiac ganglia, the majority of SP-IR varicose terminals in ICGs were also immunoreactive for CGRP (Fig. 7D–7F and 7G–7I), whereas some CGRP-IR varicose terminals did not exhibit colocalization of SP immunoreactivity. In the other areas of the atria including the auricles and the entrance area of the major veins, we also observed colocalization of SP and CGRP in axons and terminals (data not shown).

Since CGRP-IR axons and terminals were more abundant than those showing SP immunoreactivity in atrial muscles, we examined the effectiveness or sensitivity of the SP antibody. First, we used SP candidate antibodies from Abcam, Santa Cruz, and Immunostar. The Immunostar antibody that was used in the present experiment produced the strongest fluorescent labeling in cardiac ganglia and atrial muscles. Thus, it was used in the present study. Second, we followed up with an identical labeling experiment using whole-mounts of mouse small intestine as well as the aortic wall. We found that CGRP and SP antibodies

strongly labeled both axons and terminal structures in the small intestine (Fig. 8). CGRP-IR axons innervated the myenteric ganglionic plexus and formed varicose endings around individual neurons (Figure 8A and 8D), but few if any free endings in the muscle layer showed CGRP immunoreactivity (Figure 8D). In contrast, SP-IR axons terminated in the myenteric ganglionic plexus and formed varicose endings around individual neurons as well as extensive networks in the circular muscle (CM) layer (Figure 8B and 8E). Some SP-IR axons and terminals were colocalized with CGRP-IR axons and terminals (Figure 8C). Within the aortic wall, SP axons and terminals were also strongly labeled (not shown here). Thus, we believe the SP antibody can effectively label the axons and terminals in atria.

DISCUSSION

We have characterized the distribution and morphology of CGRP-IR and SP-IR axons and terminals in whole-mount preparations of the atria of mice. We found extensive networks of CGRP-IR nerve fibers and varicose terminals in both atria, and some CGRP-IR nerves formed varicose terminals around neurons of cardiac ganglia. CGRP-IR nerve fibers and varicose terminals were also present in the superior and inferior vena cava at their junctions with the atria as well as in pulmonary veins. Labeling for SP had a similar pattern, and most SP immunoreactivity was colocalized with CGRP immunoreactivity. However, axons and varicose nerve processes at all of these sites may contain CGRP but lacked SP immunoreactivity. These observations provide the neuroanatomical characterization of these neuropeptides in mouse atrial tissue and establish a structural framework for evaluating their physiological functions in murine models of cardiovascular diseases.

Origin of CGRP-IR and SP-IR axons.

Since neither CGRP nor SP occurred in neurons of the mouse ICG, the atrial nerve fibers that contain these peptides must have an extrinsic source. This conclusion agrees with results obtained in several species including guinea pigs, rats and humans (Papka and Urban, 1987; Wharton et al., 1990; Tay and Wong, 1992; Parsons 2004; Richardson et al., 2003; Hoover et al., 2009). Sensory ganglia (*i.e.*, dorsal root ganglia and/or nodose ganglia) are the most likely source of atrial CGRP and SP nerve fibers based on several lines of evidence. Colocalization of CGRP and SP in peripheral nerves is typical for a large group of primary afferent neurons that respond to nociceptive stimuli(Franco-Cereceda et al., 1987; Maggi 1995). Such neurons comprise a significant percentage of the neuronal perikarya located in the dorsal root ganglia and the vagal sensory ganglia. These neurons also contain transient receptor potential vanilloid subfamily type I (TRPV1) channels, which are known to be targets for capsaicin (Zahner et al., 2003; Pan and Chen, 2004; Price and Flores, 2007). Activation of TRPV1 channels by capsaicin causes release of CGRP and SP from afferent nerve endings. Such studies have demonstrated the ability of capsaicin to evoke release of these neuropeptides from isolated hearts and isolated atrial preparations (Saito et al., 1986; Hoover 1987; Franco-Cereceda and Liska, 2000). Based on these observations, we suggest that CGRP-IR and SP-IR nerve fibers in the mouse atria in the present study may also have a sensory origin.

Whether CGRP-IR and SP-IR nerve projections to the mouse atria originate from the dorsal root ganglia, nodose ganglia, or both sites is unknown. Previous studies of the guinea pig provided evidence that the dorsal root ganglia are the major source of CGRP-IR and SP-IR nerve fibers in the heart of that species (Dalsgaard et al., 1986; Papka and Urban, 1987). Likewise, retrograde tracer studies established that the canine ventricular myocardium received afferent projections from CGRP-IR and/or SP-IR neurons of the dorsal root ganglia but not from those of the nodose ganglion (Hoover et al., 2008). Our previous work with rats showed that vagal afferent axons from the nodose ganglion form flower-spray terminals in the atria (Cheng et al. 1997b), and this observation has been confirmed in our recent studies of vagal afferent projections to the aortic arch (Li et al. 2010) and atria in mice (unpublished). Since we did not observe any CGRP and SP-IR terminals with flower-spray morphology in the present study, it is likely that the majority of CGRP-IR and SP-IR cardiac axons were from the DRG.

Takanaga et al. (2003) reported that some cardiac motoneurons in the dorsal motor nucleus of the vagus(DmnX) contain CGRP, but no CGRP-IR neurons were identified in the external formation of the nucleus ambiguus, which is one of the major sources of vagal cardiac motoneurons. Since the DmnX projects to cardiac ganglia (Cheng et al. 1999), it is possible that some CGRP might be localized to vagal efferent fibers that project to the ICG. However, varicose contacts of CGRP-IR nerves with individual PNs were much less extensive than those of parasympathetic axons, which formed robust, dense basket endings that tightly wrap around the somata of individual PNs (Cheng et al. 1999, 2004; Ai et al. 2007a, Li et al. 2010). Furthermore, other investigators have found that neither SP nor CGRP colocalizes with cholinergic markers in the ICG (Parsons 2004; Hoover et al., 2009), which argues against a vagal efferent origin for these neuropeptides. Nevertheless, further studies are needed to test whether these CGRP and SP cardiac axons are from DRG in mice.

Innervation of CGRP-IR and SP-IR axons in the whole-mount atria of mice.

Previous studies of sectioned cardiac tissue have demonstrated the presence of CGRP-IR and SP-IR nerve fibers in discrete atrial regions of several species (Saito A et al., 1986; Parsons and Neel, 1987; Papka and Urban, 1987; Crick et al., 1994, 1999; Mousa et al., 2010). The presence of CGRP fibers and varicose terminals throughout the atria has been observed in sectioned tissues from guinea pig (Onuoha et al., 1999), pig (Crick et al., 1999) and rat (Sequira et al.,, 2005; Moussa et al., 2010). SP innervation of the endocardium and myocardium has been reported by Tay and Wong (1992) in Crabeater Macaques, in the endocardium of the human heart (Marron et al., 1994), and the coronary arteries of guinea pigs (Papka and Urban, 1987). Overall, between the species studied, CGRP/SP innervation of the cardiac layers is consistent.

In those studies employing immunohistochemistry for both CGRP and SP, significant, though not exclusive colocalization of these signals has been noted in epicardium and myocardium in human (Wharton et al., 1990; Crick et al., 1994), rat (Richardson et al., 2003; Moussa et al., 2010) and mudpuppy (Parsons et al., 1987). In addition, these publications describe a pattern of ICG innervation by varicose CGRP/SP-IR fibers with varicose fibers closely passing-by the PNs and some of them formed obvious pericellular

terminal structures, which are consistent with our present work. In studies employing only SP IHC, the identical pattern of ICG innervation by SP-IR fibers is observed in guinea pigs (Hardwick et al., 1995) and macaques Tay and Wong (1992).

Our observation that CGRP-IR nerve fibers are more abundant that SR-IR fibers in mouse atria is consistent with previous studies of dog DRG (Hoover et al., 2008) and human ICG (Hoover et al., 2009). The former study found that more canine DRG neurons stained for CGRP alone compared to those staining for SP alone and those staining for both CGRP and SP. Double labeling of human ICG for SP and CGRP showed a significant colocalization of these peptides in pericellular terminal structures, but additional fibers stained for CGRP alone. Collectively, these findings support our conclusion that some cardiac afferent nerve fibers in mouse atrial whole-mounts contain CGRP without SP.

Using dual labeling, most previous studies show that the PNs in the ICGs are neither CGRP-IR nor SP-IR. In particular, CGRP or SP immunoreactivity was not found in the PNs of humans (Wharton et al., 1990; Hoover et al., 2009), rats (Shoba et al., 2000; Richardson et al., 2003), macaque (Tay and Wong, 1992), pig (Crick et al., 1999) and mudpuppy (Parsons and Neil, 1987), which is consistent with our observation.

Though previous studies have provided many details of CGRP-IR or SP-IR axon innervation, tissue sectioning may disrupt the 3-D structure of axons and terminals, so these studies could not show the distribution and morphology of the axons and terminals over the entire atrium. In addition, sectioning of tissues makes comparison between normal and pathological tissues difficult. Although some previous studies used whole-mount preparations of cardiac tissue, these focused on the intrinsic cardiac nervous system rather than whole atrial tissues (Richardson et al., 2003; Parsons 2004). In contrast to earlier studies in other species, our work in mice presents a holistic view of CGRP-IR and SP-IR axons and differentiated terminal structures in different layers throughout the atria and associated veins, thus providing a comprehensive view or map for distribution and morphology of CGRP-IR and SP-IR axons and terminals in the mouse atria.

Considering the mouse as a model for studying cardiac sensory innervation, we found notable similarities of CGRP-IR or SP-IR axon innervation of atria in term of microscopic terminal structures in the epicardium and myocardium as well as in ICG between mouse and other species including human cardiac sensory nerve structures (Wharton et al., 1990; Crick et al., 1994; and Hoover et al., 2009). Furthermore, the mouse model enabled us to label CGRP-IR or SP-IR axon innervation and provide details of the terminal structures in the whole-mount atria due to the thinner walls of atria, producing a map for CGRP-IR or SP-IR axon innervation. This map may potentially have the following advantages over the sectioned tissues. *First*, this map enables us to follow the extrinsic large axon bundles and branches to individual terminals. In different mice, this map is very consistent with small variations. *Second*, different regions (SA, AV, and associated veins) can be easily identified, and thus the axons and terminals within these regions can be quantified and compared across different animals. *Third*, the intact microscopic axonal and terminals structures in different layers of the atria (epicardium and myocardium) can be visualized and analyzed in 3-D. These advantages may enable us to qualitatively and quantitatively compare the changes of

the distribution and morphology of these axons and terminals in normal and diseased cardiac tissues in the future.

Functional implications

The localization of CGRP and SP in varicose nerve processes in the atria, adjacent portions of the vena cava and pulmonary veins, and in the ICG suggests the possibility that these peptides can be released at these sites and have local actions. In fact, there is strong experimental evidence that CGRP/SP- containing afferent neurons can have both afferent and efferent actions (Geppetti et al., 2008). Experimental studies have demonstrated that local release of CGRP and SP can be evoked by pharmacological stimulation with capsaicin, nicotine, and several other agents (Franco-Cereceda and Liska, 2000). These nociceptive nerve fibers are also activated and release their neuropeptides when stimulated by protons and other chemicals generated during ischemia, and central release of these neuropeptides during myocardial ischemia probably contributes to the sensation of cardiac pain (Franco-Cereceda and Liska, 2000; Hoover et al., 2000). Such afferent/efferent function of axons is termed as axon-reflex (Holzer 1991; Maggi 1995; Gillespie 2005, Powley 2013). Possibly these atrial CGRP and SP axons may regulate atrial functions during ventricular ischemia (Hoover et al 2000; Zhong and Wang 2007, 2009).

Previous physiological and pharmacological studies have demonstrated that SP can act directly on cardiac ganglionic cells to cause membrane depolarization and thereby modulate cholinergic control of the heart (Hardwick et al., 1995; Hardwick et al., 1997; Hoover et al., 2000). Other studies have shown that endogenous and applied CGRP have positive chronotropic and inotropic effects on isolated atrial preparations (Saito et al., 1986). Our observation of CGRP-IR nerve fibers near pulmonary veins is particularly noteworthy since cardiomyocytes at this region have been implicated in atrial arrhythmogenesis (Chard and Tabrizchi, 2009). It is possible that local release of CGRP from these afferent fibers might influence this process. In this regard, other investigators have shown that CGRP can precondition the ventricular myocardium and thereby provide protection from ischemia/reperfusion injury (Bolli and Abdel-Latif, 2005; Wang and Wang, 2005; Li et al., 2008; Zhong and Wang, 2007) and attenuate reperfusion ventricular arrhythmias (Li et al, 1996).

Summary

In this study, we have reported a detailed documentation of the presence, distribution and morphology of CGRP-IR and SP-IR axons in the whole-mount atria of mice. These nerve fibers are most likely sensory in origin and form an extensive plexus that covers both atria, extends into adjacent pulmonary veins and the vena cava, and also sends projections into the cardiac parasympathetic ganglia. The broad and diverse distribution of these neuropeptide-containing nerve endings supports the concept that CGRP and SP have important roles in the neural control of atrial function. Previous investigators have shown that CGRP-containing nerves can have cardioprotective and antiarrhythmic influences on the ventricles during myocardial ischemia (Li et al., 1996; Li et al., 2008). We postulate that the extensive distribution of CGRP- and SP-containing nerve fibers in atrial whole-mount preparations may also have significant roles in cardiac diseases, which needs to be investigated in the future.

ACKNOWLEDGMENTS

This work was supported by NIH RO1 HL-79636, RO1AG-021020, and RO3 AG023297 to ZJC.

REFERENCE

Ai J, Epstein PN, Gozal D, Yang B, Wurster RD, Cheng ZJ, 2007a. Morphology and topography of nucleus ambiguus projections to cardiac ganglia in rats and mice. Neuroscience 149, 845–860. [PubMed: 17942236]

Ai J, Gozal D, Li L, Wead WB, Chapleau MW, Wurster RD, Yang B, Li H, Liu R, Cheng Z, 2007b. Degeneration of vagal efferent axons and terminals in cardiac ganglia of aged rats. J. Comp. Neurol 504, 74–88. [PubMed: 17614301]

Ai J, Wurster RD, Harden SW, Cheng ZJ, 2009. Vagal afferent innervation and remodeling in the aortic arch of young-adult Fischer 344 rats following chronic intermittent hypoxia. Neuroscience 164, 658–666. [PubMed: 19580847]

Becker DE, Ancin H, Szarowski DH, Turner JN, Roysam B, 1996. Automated 3-D montage synthesis from laser-scanning confocal images: application to quantitative tissue-level cytological analysis. Cytometry 25, 235–245. [PubMed: 8914820]

Benemei S, Nicoletti P, Capone JG, Geppetti P, 2009. CGRP receptors in the control of pain and inflammation. Curr. Opin. Pharmacol 9, 9–14. [PubMed: 19157980]

Bolli R, Abdel-Latif A, 2005. No pain, no gain: the useful function of angina. Circulation 112, 3541–3543. [PubMed: 16330693]

Chard M, Tabrizchi R, 2009. The role of pulmonary veins in atrial fibrillation: a complex yet simple story. Pharmacol. Ther 124, 207–218, [PubMed: 19628005]

Cheng Z, Zhang H, Guo SZ, Wurster RD, Gozal D, 2004. Differential control over postganglionic neurons in rat cardiac ganglia by NA and DmnX neurons: anatomical evidence. Am. J. Physiol. Regul. Integr. Comp. Physiol 286, R625–633. [PubMed: 14644755]

Cheng Z, Powley TL, 2000. Nucleus ambiguus projections to cardiac ganglia of rat atria: an anterograde tracing study. J. Comp. Neurol 424, 588–606. [PubMed: 10931483]

Cheng Z, Powley TL, Schwaber JS, Doyle FJ 3rd. 1999. Projections of the dorsal motor nucleus of the vagus to cardiac ganglia of rat atria: an anterograde tracing study. J. Comp. Neurol 410, 320–41, [PubMed: 10414536]

Cheng Z, Powley TL, Schwaber JS, Doyle FJ 3rd. 1997a. Vagal afferent innervation of the atria of the rat heart reconstructed with confocal microscopy. J. Comp. Neurol 381, 1–17. [PubMed: 9087415]

Cheng Z, Powley TL, Schwaber JS, Doyle FJ 3rd. 1997b. A laser confocal microscopic study of vagal afferent innervation of rat aortic arch: chemoreceptors as well as baroreceptors. J. Auton. Nerv. Syst 67, 1–14. [PubMed: 9470139]

Collins TJ, 2007. Image J for microscopy. Biotechniques 43, 25–30.

Crick SJ, 1994. Wharton J, Sheppard MN, Royston D, Yacoub MH, Anderson RH, Polak JM, Innervation of the human cardiac conduction system. A quantitative immunohistochemical and histochemical study. Circulation 89, 1697–1708. [PubMed: 7908612]

Crick SJ, Sheppard MN, Ho SY, Anderson RH, 1999. Localisation and quantitation of autonomic innervation in the porcine heart I: conduction system. J. Anat 195 (Pt 3), 341–373. [PubMed: 10580850]

Dalsgaard CJ, Franco-Cereceda A, Saria A, Lundberg JM, Theodorsson-Norheim E, Hökfelt T, 1986. Distribution and origin of substance P and neuropeptide Y-immunoreactive nerves in the guinea-pig heart. Cell Tissue Res. 243, 477–485. [PubMed: 2420458]

Epstein PN, Overbeek PA, Means AR, 1989. Calmodulin-induced early-onset diabetes in transgenic mice. Cell 58, 1067–1073. [PubMed: 2673540]

Fox EA, Phillips RJ, Martinson FA, Baronowsky EA, Powley TL, 2000. Vagal afferent innervation of smooth muscle in the stomach and duodenum of the mouse: morphology and topography. J. Comp. Neurol 428, 558–576. [PubMed: 11074451]

Franco-Cereceda A, Liska J, 2000. Potential of calcitonin gene-related peptide in coronary heart disease. Pharmacology 60, 1–8. [PubMed: 10629436]

Franco-Cereceda A, Henke H, Lundbery JM, Petermann JB, Hökfelt T, Fischer JA, 1987. Calcitonin gene-related peptide (CGRP) in capsaicin-sensitive substance P-immunoreactive sensory neurons in animals and man: Distribution and release by capsaicin. Peptides 8, 399–410. [PubMed: 2438668]

Geppetti P, Nassini R, Materazzi S, Benemei S, 2008. The concept of neurogenic inflammation. BJU. Int 101 Suppl 3, 2–6.

Gillespie JI, 2005. Inhibitory actions of calcitonin gene-related peptide and capsaicin: evidence for local axonal reflexes in the bladder wall. BJU. Int 95, 149–156. [PubMed: 15638914]

Gu H, Zhang ZH, Epstein PN, Li L, Harden SW, Wurster RD, Cheng ZJ, 2009. Impaired baroreflex control of renal sympathetic nerve activity in type 1 diabetic mice (OVE26). Neuroscience 161, 78–85. [PubMed: 19303918]

Gu H, Epstein PN, Li L, Wurster RD, Cheng ZJ, 2008. Functional changes in baroreceptor afferent, central and efferent components of the baroreflex circuitry in type 1 diabetic mice (OVE26). Neuroscience 152, 741–752. [PubMed: 18328631]

Hardwick JC, Mawe GM, Parsons RL, 1997. Tachykinin-induced activation of nonspecific cation conductance via NK3 neurokinin receptors in guinea-pig intracardiac neurones. J. Physiol 504 (Pt 1), 65–74. [PubMed: 9350618]

Hardwick JC, Mawe GM, Parsons RL, 1995. Evidence for afferent fiber innervation of parasympathetic neurons of the guinea-pig cardiac ganglion. J. Auton. Nerv. Syst 53, 166–174. [PubMed: 7560753]

Holzer P, 1991. Capsaicin: cellular targets, mechanisms of action, and selectivity for thin sensory neurons. Pharmacol. Rev 43, 143–201. [PubMed: 1852779]

Hongbao M, Yan Y, and Shen C, 2009. Gender-specific effects of calcitonin gene-related peptide and substance P on coronary blood flow in an experimental model. Angiology 60, 569–575. [PubMed: 19017671]

Hoover DB, 1987. Effects of capsaicin on release of substance P-like immunoreactivity and physiological parameters in isolated perfused guinea-pig heart. Eur. J. Pharmacol 141, 489–492. [PubMed: 2444445]

Hoover DB, Chang Y, Hancock JC, Zhang L, 2000. Actions of tachykinins within the heart and their relevance to cardiovascular disease. Jpn. J. Pharmacol 84, 367–373. [PubMed: 11202607]

Hoover DB, Shepherd AV, Southerland EM, Armour JA, Ardell JL, 2008. Neurochemical diversity of afferent neurons that transduce sensory signals from dog ventricular myocardium. Auton. Neurosci 141, 38–45. [PubMed: 18558516]

Hoover DB, Isaacs ER, Jacques F, Hoard JL, Page P, Armour JA, 2009. Localization of multiple neurotransmitters in surgically derived specimens of human atrial ganglia. Neuroscience 164, 1170–1179. [PubMed: 19747529]

Ieda M, Kanazawa H, Ieda Y, Kimura K, Matsumura K, Tomita Y, Yagi T, Onizuka T, Shimoji K, Ogawa S, Makino S, Suno M, Fukuda K, 2006. Nerve growth factor is critical for cardiac sensory innervation and rescues neuropathy in diabetic hearts. Circulation 114, 2351–2363. [PubMed: 17101855]

Kunz TH, Scott M, Ittner LM, Fischer JA, Born W, Vogel J 2007. Calcitonin gene-related peptide-evoked sustained tachycardia in calcitonin receptor-like receptor transgenic mice is mediated by sympathetic activity. Am. J. Physiol. Heart. Circ. Physiol 293, H2155–H2160. [PubMed: 17660394]

Li D, Li NS, Chen QQ, Guo R, Xu PS, Deng HW, Li YJ, 2008. Calcitonin gene-related peptide-mediated cardioprotection of postconditioning in isolated rat hearts. Regul. Pept 147, 4–8. [PubMed: 18166234]

Li YJ, Xiao ZS, Peng CF, Deng HW, 1996. Calcitonin gene-related peptide-induced preconditioning protects against ischemia-reperfusion injury in isolated rat hearts. Eur. J. Pharmacol 311, 163–167. [PubMed: 8891596]

Li L, Huang C, Ai J, Yan B, Gu H, Ma Z, Li AY, Xinyan S, Harden SW, Hatcher JT, Wurster RD, Cheng ZJ, 2010. Structural remodeling of vagal afferent innervation of aortic arch and nucleus ambiguus (NA) projections to cardiac ganglia in a transgenic mouse model of type 1 diabetes (OVE26). J. Comp. Neurol 518, 2771–2793. [PubMed: 20506475]

Lin M, Hatcher JT, Chen QH, Wurster RD, Li L, Cheng ZJ, 2011. Maternal diabetes increases large conductance Ca^{2+}-activated K^+ outward currents that alter action potential properties but do not contribute to attenuated excitability of parasympathetic cardiac motoneurons in the nucleus ambiguus of neonatal mice. Am. J. Physiol. Regul. Integr. Comp. Physiol 300, R1070–1078. [PubMed: 21248308]

Lin M, Chen QH, Wurster RD, Hatcher JT, Liu YQ, Li L, Harden SW, Cheng ZJ, 2010a. Maternal diabetes increases small conductance Ca^{2+}-activated K^+ (SK) currents that alter action potential properties and excitability of cardiac motoneurons in the nucleus ambiguus. J. Neurophysiol 104, 2125–2138. [PubMed: 20668269]

Lin M, Harden SW, Li L, Wurster RD, Cheng ZJ, 2010b. Impairment of baroreflex control of heart rate in conscious transgenic mice of type 1 diabetes (OVE26). Auton. Neurosci 152, 67–74. [PubMed: 19910264]

Lin M, Ai J, Li L, Huang C, Chapleau MW, Liu R, Gozal D, Wead WB, Wurster RD, Cheng ZJ, 2008. Structural remodeling of nucleus ambiguus projections to cardiac ganglia following chronic intermittent hypoxia in C57BL/6J mice. J. Comp. Neurol 509, 103–117. [PubMed: 18425809]

Maggi CA, 1995. Tachykinins and calcitonin gene-related peptide (CGRP) as co-transmitters released from peripheral endings of sensory nerves. Prog Neurobiol 45, 1–98. [PubMed: 7716258]

Marron K, Wharton J, Sheppard MN, Gulbenkian S, Royston D, Yacoub MH, Anderson RH, Polak JM, 1994. Human endocardial innervation and its relationship to the endothelium: an immunohistochemical, histochemical, and quantitative study. Cardiovasc. Res 28, 1490–1499. [PubMed: 8001036]

Mousa SA, Shaqura M, Schaper J, Huang W, Treskatsch S, Habazettl H, Abdul-Khaliq H, Schafer M, 2010. Identification of mu- and kappa-opioid receptors as potential targets to regulate parasympathetic, sympathetic, and sensory neurons within rat intracardiac ganglia. J. Comp. Neurol 518, 3836–3847. [PubMed: 20653037]

Onuoha GN, Alpar EK, Nicholls DP, Buchanan KD, 1999. Calcitonin gene-related peptide, neuropeptide Y and atrial natriuretic peptide distribution in guinea pig heart from paraffin wax-embedded and formalin-cryoprotected tissues. Histochem. J 31, 617–621. [PubMed: 10579631]

Pan HL, Chen SR, 2004. Sensing tissue ischemia: another new function for capsaicin receptors? Circulation 110, 1826–1831. [PubMed: 15364816]

Papka RE Urban L, 1987. Distribution, origin and sensitivity to capsaicin of primary afferent substance P-immunoreactive nerves in the heart. Acta Physiol. Hung 69, 459–468. [PubMed: 2444072]

Parsons RL, 2004. Mammalian cardiac ganglia as local integration centers: Histochemical and electrophysiological evidence. In: Dun NJ, Machado BH, and Pilowsky PM (Eds.), Neural Mechanisms of Cardiovascular Regulation. Kluwer Academic Publishers, Boston, pp. 335–356.

Parsons RL, Neel DS, 1987. Distribution of calcitonin gene-related peptide immunoreactive nerve fibers in the mudpuppy cardiac septum. J. Auton. Nerv. Syst 21, 135–43. [PubMed: 2453547]

Powley TL, 2013. Central control of autonomic functions: organization of the autonomic nervous system. In: Fundamental Neuroscience 4th edition by: Squire LR et al. Elsevier. pp 730–749.

Price TJ, Flores CM, 2007. Critical evaluation of the colocalization between calcitonin gene-related peptide, substance P, transient receptor potential vanilloid subfamily type 1 immunoreactivities, and isolectin B4 binding in primary afferent neurons of the rat and mouse. J. Pain 8, 263–272. [PubMed: 17113352]

Richardson RJ, Grkovic I, Anderson CR, 2003. Immunohistochemical analysis of intracardiac ganglia of the rat heart. Cell Tissue Res. 314, 337–350. [PubMed: 14523644]

Saito A, Kimura S, Goto K, 1986. Calcitonin gene-related peptide as potential neurotransmitter in guinea pig right atrium. Am. J. Physiol 250: H693–698. [PubMed: 2870646]

Sampaio KN, Mauad H, Spyer KM, Ford TW, 2003. Differential chronotropic and dromotropic responses to focal stimulation of cardiac vagal ganglia in the rat. Exp. Physiol 88, 315–27. [PubMed: 12719756]

Sequeira IM, Haberberger RV, Kummer W, 2005. Atrial and ventricular rat coronary arteries are differently supplied by noradrenergic, cholinergic and nitrergic, but not sensory nerve fibres. Ann. Anat 187, 345–355. [PubMed: 16163847]

Shoba T, Tay SS, 2000. Nitrergic and peptidergic innervation in the developing rat heart. Anat. Embryol. (Berl) 201, 491–500. [PubMed: 10909903]

Song JX, Wang LH, Yao L, Xu C, Wei ZH, Zheng LR, 2009. Impaired transient receptor potential vanilloid 1 in streptozotocin-induced diabetic hearts. Int. J. Cardiol 134, 290–292. [PubMed: 18378339]

Takanaga A, Hayakawa T, Tanaka K, Kawabata K, Maeda S, Seki M, 2003. Immunohistochemical characterization of cardiac vagal preganglionic neurons in the rat. Auton. Neurosci 106, 132–137. [PubMed: 12878082]

Tay SS, Wong WC, 1992. Immunocytochemical localisation of substance P-like nerves in the cardiac ganglia of the monkey (Macacafascicularis). J. Anat 180 (Pt 2), 239–245. [PubMed: 1380495]

Thévenaz P, Unser M, 2007. User-friendly semiautomated assembly of accurate image mosaics in microscopy. Microsc. Res. Tech 70, 135–146. [PubMed: 17133410]

Thornton E, Ziebell JM, Leonard AV, Vink R, 2010. Kinin receptor antagonists as potential neuroprotective agents in central nervous system injury. Molecules 15: 6598–6618. [PubMed: 20877247]

Wang L, Wang DH, 2005. TRPV1 gene knockout impairs postischemic recovery in isolated perfused heart in mice. Circulation 112, 3617–3623. [PubMed: 16314376]

Wei Z, Wang L, Han J, Song J, Yao L, Shao L, Sun Z, Zheng L, 2009. Decreased expression of transient receptor potential vanilloid 1 impairs the postischemic recovery of diabetic mouse hearts. Circ. J 73, 1127–1132. [PubMed: 19372621]

Wharton J, Polak JM, Gordon L, Banner NR, Springall DR, Rose M, Khagani A, Wallwork J, Yacoub MH, 1990. Immunohistochemical demonstration of human cardiac innervation before and after transplantation. Circ. Res 66, 900–912. [PubMed: 2317894]

Yan B, Li L, Harden SW, Epstein PN, Wurster RD, Cheng ZJ, 2009. Diabetes induces neural degeneration in nucleus ambiguus (NA) and attenuates heart rate control in OVE26 mice. Exp. Neurol 220, 34–43. [PubMed: 19615367]

Zahner MR, Li DP, Chen SR, Pan HL, 2003. Cardiac vanilloid receptor 1expressing afferent nerves and their role in the cardiogenic sympathetic reflex in rats. J. Physiol 551, 515–523. [PubMed: 12829722]

Zheng S, Huang Y, Yang L, Chen T, Xu J, Epstein PN, 2011. Uninephrectomy of diabetic OVE26 mice greatly accelerates albuminuria, fibrosis, inflammatory cell infiltration and changes in gene expression. Nephron Exp. Nephrol 119, 21–32.

Zhong B, Wang DH, 2007. TRPV1 gene knockout impairs preconditioning protection against myocardial injury in isolated perfused hearts in mice. Am. J. Physiol. Heart. Circ. Physiol 293, H1791–1798. [PubMed: 17586621]

Zhong B, Wang DH, 2009, Protease-activated receptor 2-mediated protection of myocardial ischemia-reperfusion injury: role of transient receptor potential vanilloid receptors. Am. J. Physiol. Regul. Integr. Comp. Physiol 297, R1681–1690. [PubMed: 19812353]

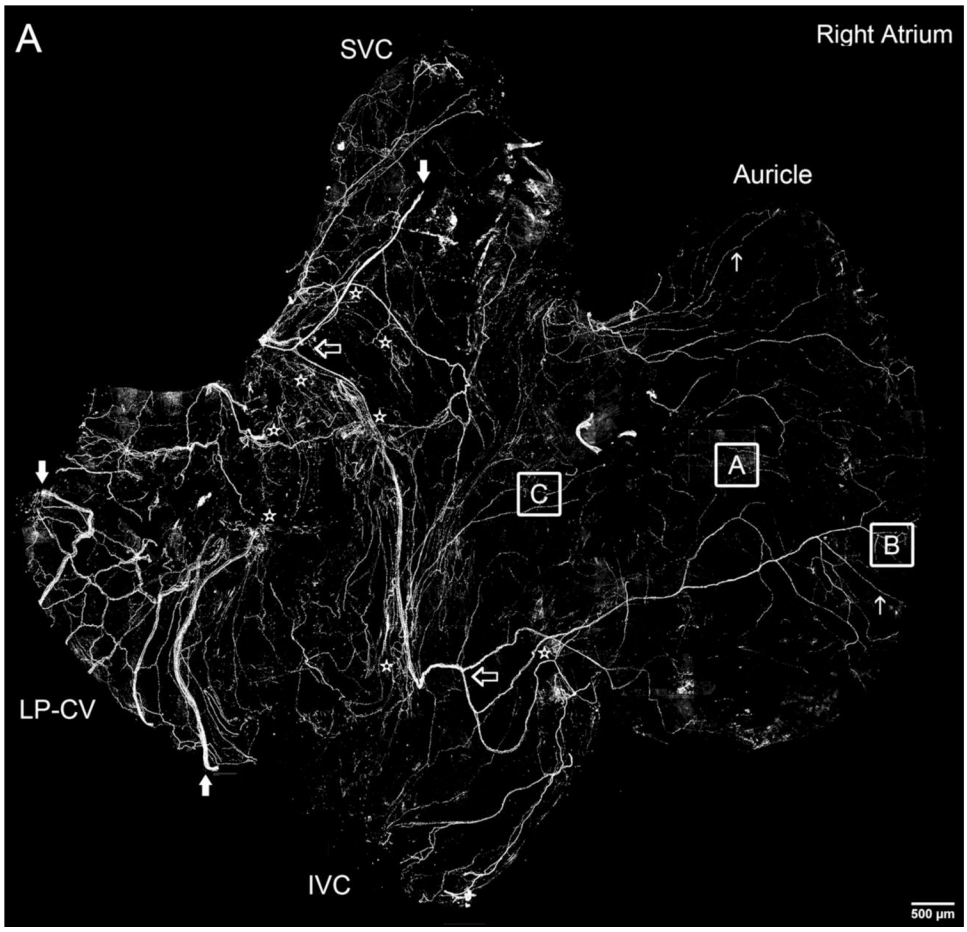

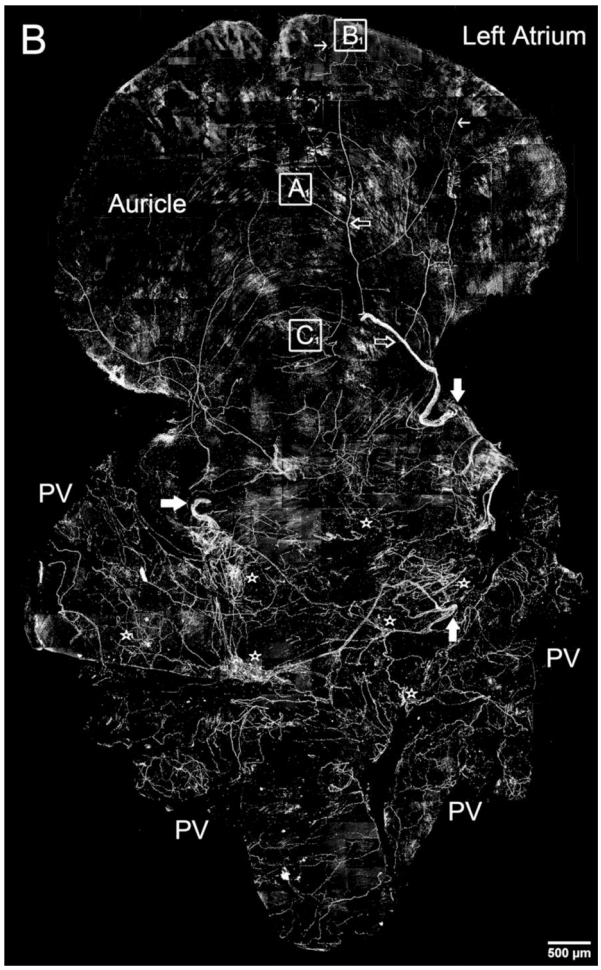

Figure 1.

Montage of all-in-focus maximum confocal projections showing distribution of CGRP-IR nerve fibers in the right and left atrium of a FVB mouse.

A. A few large CGRP-IR axon bundles (indicated by large solid arrows) entered the right atrium from SVC and LP-CV. Then, they bifurcated into small bundles (indicated by large open arrows) and single axons (indicated by small arrows). Finally, these single axons covered all regions of the atrium with terminal networks (see Figures 2 and 3 for detail), including the auricle and the entrance area of IVC, SVC and LP-CV. In addition, CGRP-IR axons innervated multiple ICGs with varicose endings around individual cardiac ganglionic principal neurons as indicated by stars (see Figures 2 and 5 for detail). Inferior vena cava: IVC; superior vena cava: SVC; left precaval vein; LP-CV.

B. A few large CGRP-IR axon bundles (indicated by large solid arrows) entered the left atrium from left and right PVs. Then, they bifurcated into small bundles (indicated by large open arrows) and single axons (indicated by small arrows). Finally, these single axons covered all regions of the atrium with terminal networks (see Figures 2 and 3 for detail), including the auricle and the entrance area of PVs (Figure 4). In addition, CGRP-IR axons innervated multiple ICGs with varicose endings around individual cardiac ganglionic principal neurons as indicated by stars (see Figures 2 and 5 for detail). Pulmonary veins:

PVs. Note: Since panels A and B are confocal montages which show the overall distribution of CGRP-IR axons, the detail structures of the axons and terminals are not visible at this magnification. The square frames A, B, and C and A_1, B_1, and C_1 are the sampling windows where the detail structure of axon terminals will be presented in Figure 3.Scale bars: 500 μm. *Note: If you are viewing the electronic version, please"zoom" in on these montages and view the details of axons, terminals and ganglia.*

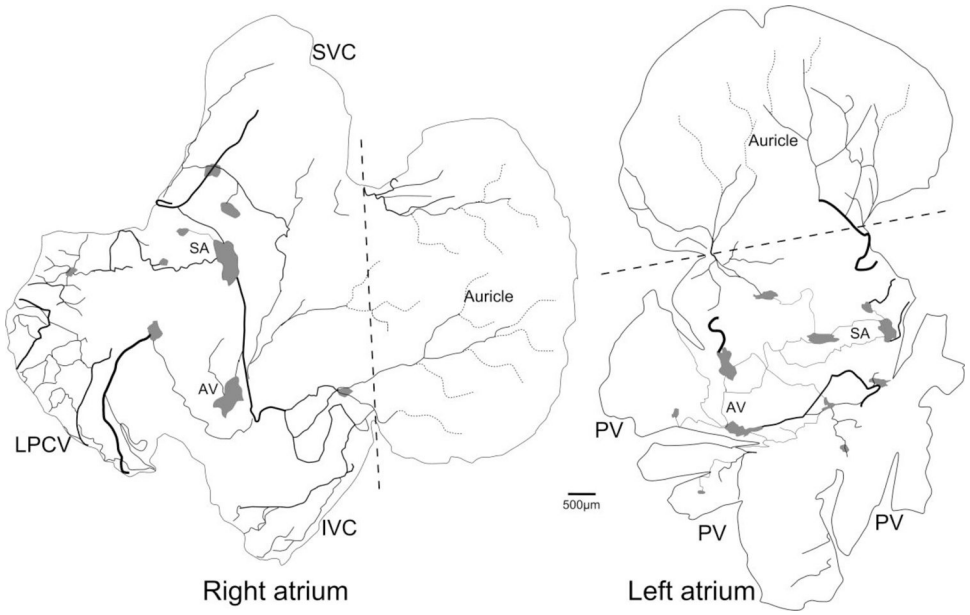

Figure 2.

Schematic drawings depicting CGRP-IR innervation of the whole-mount right and left atria in the FVB mouse as shown in Figures 1.

Each atrium was divided into an auricle region and the rest of the atrium including the entrance of the large veins. The boundary is indicated by a dotted straight line. Large bundles of CGRP-IR axons (thick lines) entered the atrium and then bifurcated into small bundles (thin lines) and ultimately the single axons (dotted lines) with terminal networks and free endings (not shown at this magnification). Both atria contained multiple intrinsic cardiac ganglia as indicated by grey areas. Sino-atrial node region: SA; atrio-ventricular node region: AV; inferior vena cava: IVC; superior vena cava: SVC; left precaval vein: LP-CV; pulmonary veins: PVs. Scale bar: 500μm.Note: intrinsic cardiac ganglionic plexuses may include 15–20 ganglia on the dorsal surface of both atria. The SA and AV nodes are in the right atria. During tissue dissection, several SA regional ganglia which had originally been connected with each other by axons were disconneted. After tissue dissection, these SA regional ganglia could be located on the dorsal surface of both left and right atria. The function roles of these individual ganglia in the SA region have been explored (Sampaio et al. 2003).

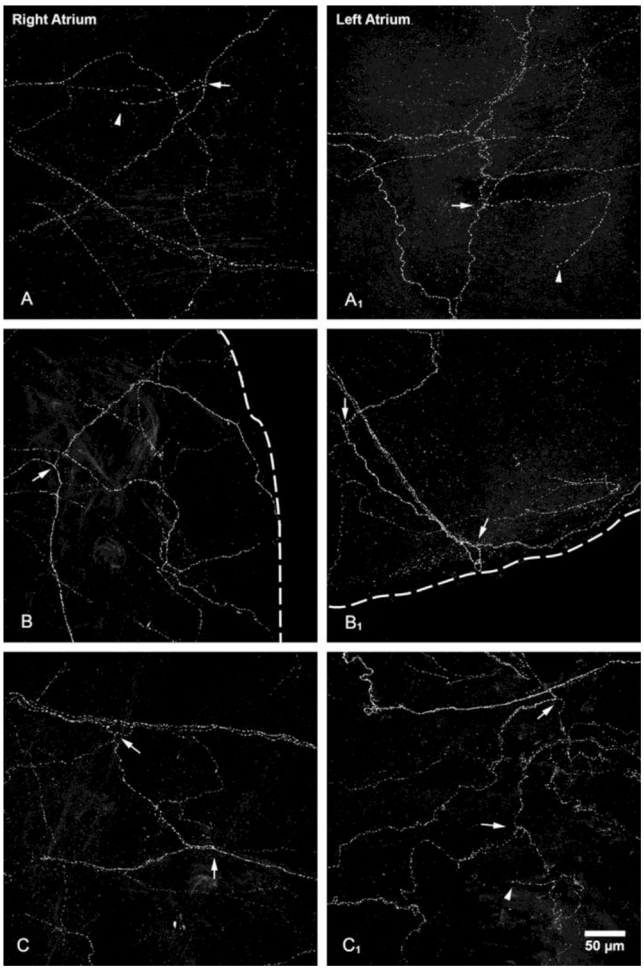

Figure 3.

CGRP-IR axons and terminals in the atria.

All-in-focus projections at the regions indicated by A, B, and C in the right atrium and A_1, B_1, and C_1 in the left atrium in Figure 1A and 1B, respectively. Detailed structure of CGRP-IR axons in different atrial regions showed similar patterns. Multiple single axon fibers formed terminal end-nets with free endings in the epicardium and myocardium. Arrows: branching points; arrow heads: free endings. Scale bar: 50μm.

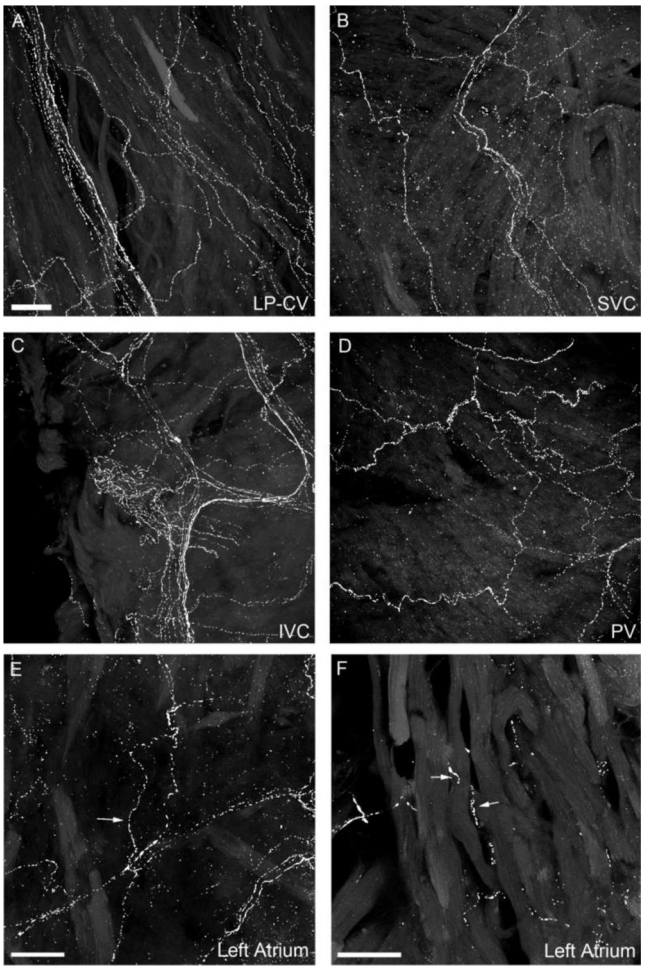

Figure 4.

CGRP-IR axons in the entrance area of the major veins.

All-in-focus projection images of LP-CV (left precaval vein; A), SVC (superior vena cava, B), IVC (inferior vena cava, C) of the right atrium; and PV (pulmonary vein, D) of the left atrium. The bright signal represents CGRP-IR axons and the dim background represents autofluorescent background from muscle layers. CGRP-IR axons in the veins exhibited similar structure of terminal end-nets and free endings as seen in the atria. E: A partial projection of confocal optically-sectioned images showing several axons (arrows) traveling in the epicardium. F: A single optical section showing that delicate CGRP axons (arrows) are in the myocardium and have close contacts with cardiomyocytes. Scale bars in A: 50 μm for A-D; in E and F: 30 μm.

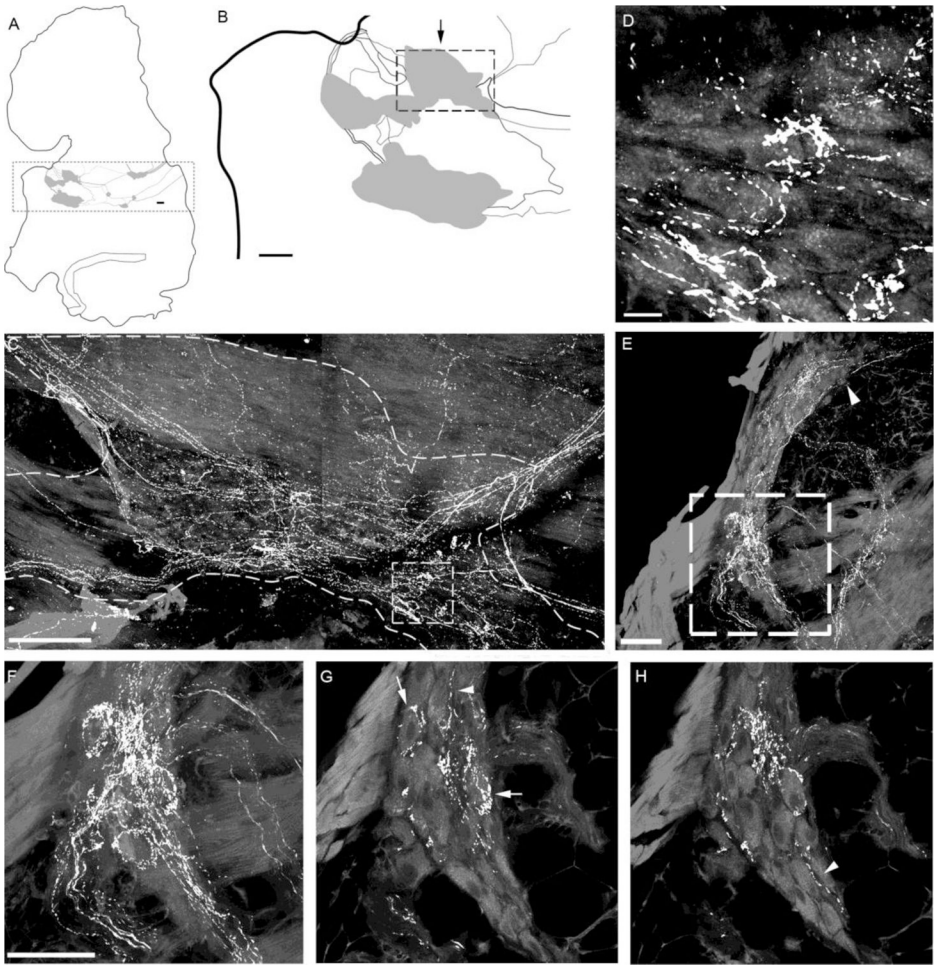

Figure 5.

CGRP-IR innervation of intrinsic cardiac ganglia (ICGs) in the atria of a representative mouse.

A. Schematic drawing of the left atrium with ICGs indicated by grey patches. The dotted frame encloses ICG plexuses. B. The ICGs at the left portion as enclosed in the dotted frame in panel A were shown at higher magnification. C. A confocal projection of the ganglion region indicated by the arrow above the dotted frame in panel B. CGRP-IR axons innervated ICG neurons (autofluorescence). Varicose CGRP-IR axons traveled in the connective between ICGs. Most of these varicose axons coursed through and passed by the ganglion, whereas some formed varicose terminals around cardiac ganglionic principal neurons (PNs). D. Higher magnification of the boxed area in C showing such axonal varicosities near PNs. Noticeably, none of PNs were CGRP-IR. E. All-in-focus projection image at the AV region of the right atrium. A ganglion is identified within the dotted frame. F. High magnification of the region with the dotted frame in panel E. G-H. Two different single optical sections showing that CGRP-IR axons formed varicosities around the individual PNs (arrows). Arrowheads in E, G, and H indicate CGRP-IR axons were passing by ICG PNs. Scale bars: 200 μm in panel B; 100 μm in panel C; 10 μm in panel D. 50 μm in panel E; 50μm in F for F-H.

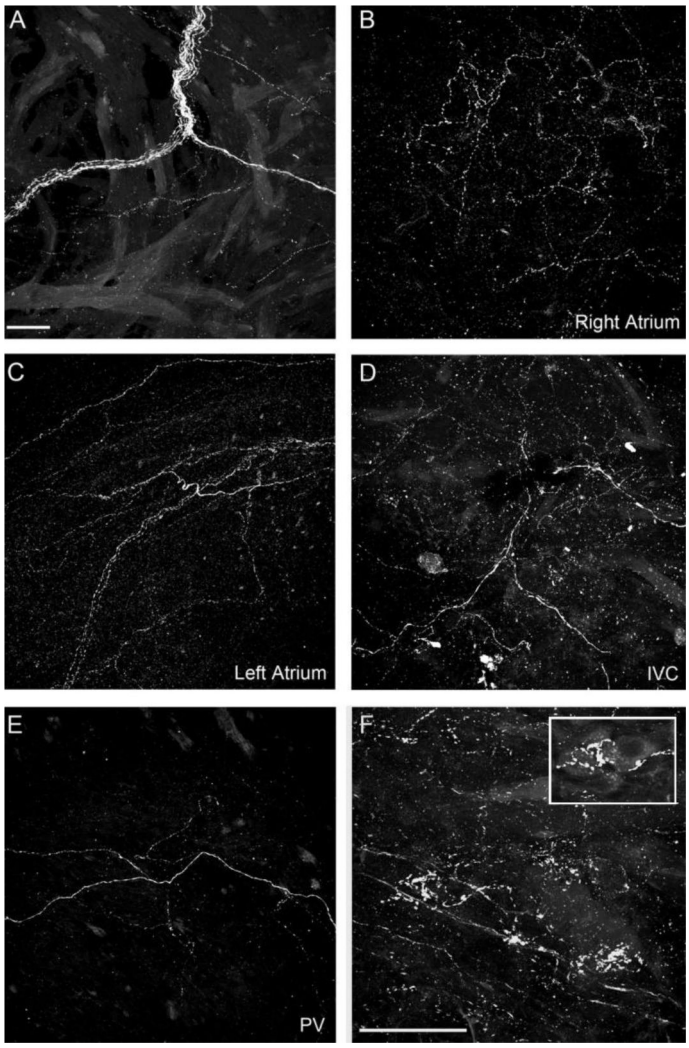

Figure 6.

SP-IR axons in atria.

A. SP-IR axon bundle in the right atrium. B. SP-IR terminal end-net in the right atrium. C. SP-IR terminal end-net in the left atrium. D. SP-IR axons in the IVC. E. SP-IR axons in a PV. F. SP-IR axons formed varicose endings around ICG PNs. The inset reveals a few gangion cells and varicose terminals around the somata of these cells. Scale bar in A: 50μm for A-E; Scale bar in F: 50μm.

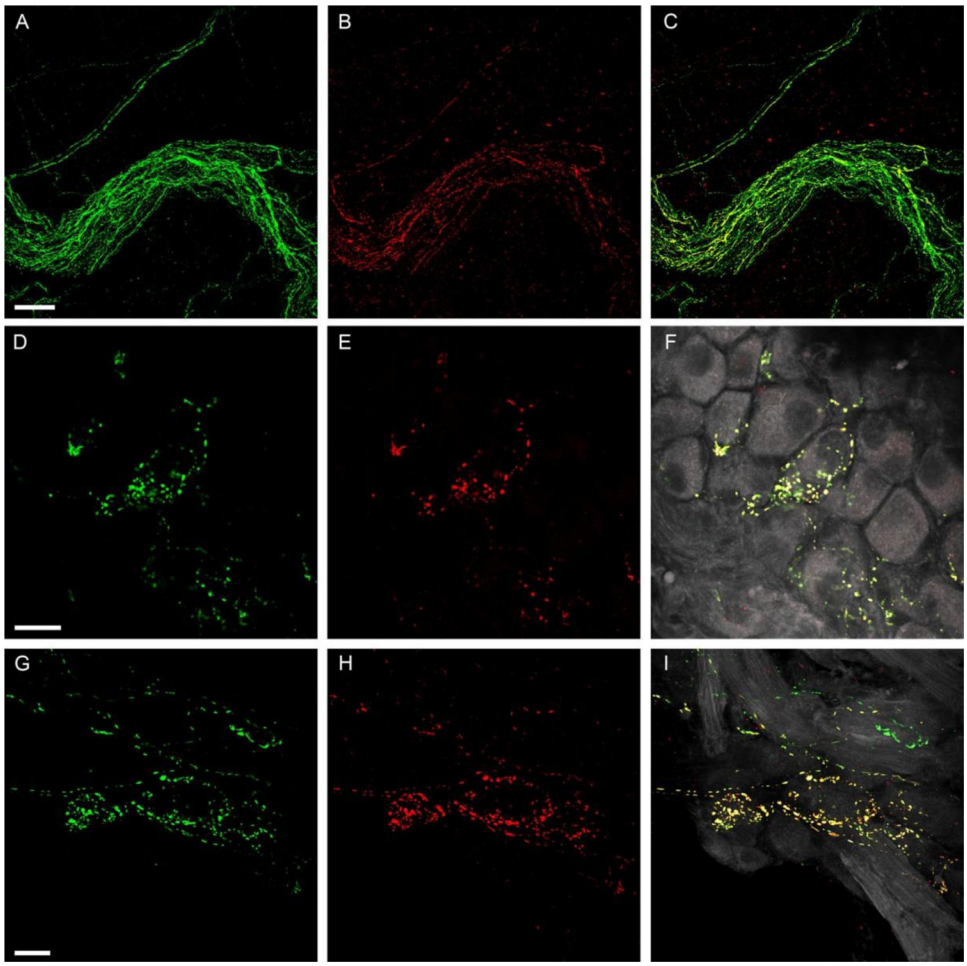

Figure 7.

Colocalization of SP-IR and CGRP-IR in axon bundles and ICGs.

A-C: Colocalization of SP-IR and CGRP-IR in an axon bundle. A large axon bundle entered the right atrium and most SP-IR (B, Red) fibers were found to have colocalization of CGRP-IR (A, Green), indicating coexpression of CGRP with SP (C,Yellow in the merged image). D-F and G-I: Two examples of colocalization of SP-IR and CGRP-IR in ICGs. Single confocal optic images show CGRP-IR terminal varicosities (D or G). Single confocal optic images show SP-IR terminal varicosites (E or H). The merged images of panel D (or G) withpanel E (or H) is shown in F (or I). PNs are in gray color. Most SP-IR varicose terminals show colocalization of CGRP-IR in their terminal varicosities. Colocalization of SP and CGRP in these terminals is signified by yellow in the composite image. Varicosities in pure green (CGRP-IR) color in panel F or I suggest that although most SP-IR fibers show colocalized CGRP expression, some fibers show exclusive CGRP immunoreactivity. Scale bars in A: 50μm for A-C, in D: 50μm for D-F, in G: 50μm for G-I.

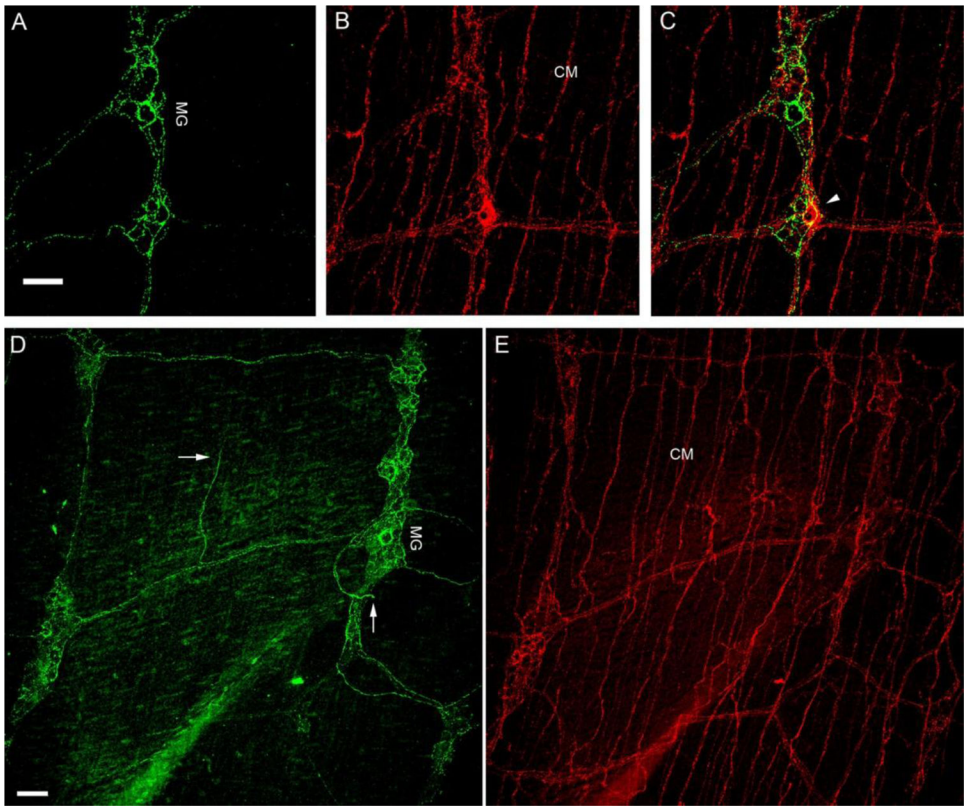

Figure 8.

CGRP-IR and SP-IR axons and terminals in the small intestine of a FVB mouse.

A, B. Single confocal optic sectioned images show CGRP-IR (Green; panel A) and SP-IR (Red; panel B) fibers and terminals in the small intestine. C. Only a few varicosities showed colocalized CGRP-IR and SP-IR in MG as yellow (arrowhead) in the composite image, whereas the majority did not. D, E. All-in-focus projection confocal images showed CGRP-IR axon terminals were mostly in MG and only a few free terminals were in the muscle layer (arrows). On the other hand, SP-IR axon networks were found richly in CM and SP-IR axon terminals were found in MG. myenteric ganglia: MG; circular muscle: CM. Scale bar in A: 50μm for A-C, in D: 50μm for D-E.

Table 1:

Antibodies Used

Antibody	Concentration	Host	Company	Emission
Anti-CGRP†	1 μl/ml	Goat	Abcam	n/a
Anti-SP†	2 μl/ml	Rabbit	Immunostar	n/a
Alexa Fluor Anti-Goat††	24 μl/ml	Donkey	Invitrogen	594 nm
Alexa Fluor Anti-Rabbit††	24 μl/ml	Donkey	Invitrogen	660 nm*

† primary

†† secondary

* infrared fluorophores are invisible to human eyes